**PASJ:** Publ. Astron. Soc. Japan , 1–??, vol. 63, Subaru special issue
© 2011. Astronomical Society of Japan.

arXiv:1101.4340v1 [astro-ph.CO] 23 Jan 2011

# Outflow in Overlooked Luminous Quasar: Subaru Observations of AKARI J1757+5907 *

Kentaro Aoki,[1] Shinki Oyabu,[1,2] Jay P. Dunn,[3] Nahum Arav,[3] Doug Edmonds,[3] Kirk T. Korista,[4] Hideo Matsuhara,[5]
and
Yoshiki Toba[5]

[1] *Subaru Telescope, National Astronomical Observatory of Japan, 650 North A'ohoku Place, Hilo, HI 96720, U.S.A.*
[2] *Graduate School of Science, Nagoya University, Chikusa-ku, Nagoya 464-8602*
[3] *Department of Physics, Virginia Tech, Blacksburg, VA 24061, U.S.A.*
[4] *Department of Physics, Western Michigan University, Kalamazoo, MI 49008-5252, U.S.A.*
[5] *Institute of Space and Astronautical Science, Japan Aerospace Exploration Agency, 3-1-1 Yoshinodai, Sagamihara, Kanagawa 229-8510*

(Received 2010 September 10; accepted 2011 January 14)

**Abstract**

We present Subaru observations of the newly discovered luminous quasar AKARI J1757+5907, which shows an absorption outflow in its spectrum. The absorption consists of 9 distinct troughs, and our analysis focuses on the troughs at $\sim -1000$ km s$^{-1}$ for which we can measure accurate column densities of He I*, Fe II and Mg II. We use photoionization models to constrain the ionization parameter, total hydrogen column density, and the number density of the outflowing gas. These constraints yield lower limits for the distance, mass flow rate and kinetic luminosity for the outflow of 3.7 kpc, 70 $M_\odot$ yr$^{-1}$, and $2.0\times10^{43}$ ergs s$^{-1}$, respectively. Such mass flow rate value can contribute significantly to the metal enrichment of the intra-cluster medium. We find that this moderate velocity outflow is similar to those recently discovered in massive post-starburst galaxies. Finally, we describe the scientific potential of future observations targeting this object.

**Key words:** galaxies: active—quasars: absorption lines—quasars: emission lines—quasars: individual (AKARI-IRC-V1 J1757000+590759)

## 1. Introduction

Roughly 20% of all quasars exhibit Broad Absorption Lines (BAL) in their spectrum (Knigge et al. 2008; Hewett & Foltz 2003), which are indicative of outflows with velocities $\sim 10^3 - 10^4$ km s$^{-1}$. Kinetic energy and mass emanating from quasars have become key elements in theoretical modeling of the evolution of supermassive black holes (SMBH) and their host galaxies (e.g., Di Matteo et al. 2005; Hopkins et al. 2008), the suppression of cooling flows in clusters (e.g., Ciotti et al. 2010; Brüggen & Scannapieco 2009), and enrichment of the intra-cluster and inter-galactic media with metals (e.g., Moll et al. 2007). Collectively, harnessing quasars' mechanical energy to help in driving the above processes is known as "AGN feedback".

To assess the contribution of BAL outflows to AGN feedback scenarios, it is (at least) necessary to determine their mass flow rate ($\dot{M}_{out}$) and kinetic luminosity ($\dot{E}_k$). Early attempts to do so were done by de Kool et al. (2001), de Kool et al. (2002), Hamann et al. (2001), and Wampler, Chugai, Petitjean (1995). Recently, using improvements in analysis methods and in target selection (see discussions in Arav et al. 2008; Dunn et al. 2010), we published several more accurate determinations of these quantities (Moe et al. 2009; Dunn et al. 2010; Bautista et al 2010; Arav et al 2010). Here we present a similar analysis of an outflow in a luminous overlooked quasar.

We use the term "BAL outflow" to designate intrinsic absorption detected in the spectrum of a quasar (i.e., originating from outflowing material in the vicinity of the AGN, see Barlow & Sargent 1997). The original BAL definition (Weymann et al. 1991) was created to differentiate, in low-resolution spectra, AGN outflow absorption systems from intervening absorbers that do not have a dynamical connection to the AGN and is now physically obsolete. Significant number of narrower absorption lines show intrinsic natures, i.e., time variability and partial coverage of the background light source. The frequency of intrinsic absorption lines are discussed and summarized in Ganguly & Brotherton (2008). We therefore use "BAL outflow" to designate the physical nature, rather than the observational definition, of the phenomenon.

AKARI-IRC-V1 J1757000+590759 (hereafter AKARI J1757+5907) was discovered during the follow-up observations of AKARI mid-infrared (MIR) All-Sky Survey. The infrared satellite AKARI performed an

* Based on data collected at Subaru Telescope, which is operated by the National Astronomical Observatory of Japan.

all-sky survey at 9 and 18 $\mu$m as well as at four far-infrared bands (Murakami et al. 2007; Ishihara et al. 2010). The initial identification of the AKARI MIR All-Sky Survey sources involved association with the Two Micron All Sky Survey (2MASS) catalog (Skrutskie et al. 2006). This search identified some AKARI MIR sources with $F(9\mu\mathrm{m})/F(Ks) > 2$ in the high galactic latitude ($|b| > 20^\circ$) after excluding the sample in the Large and Small Magellanic Clouds. AKARI J1757+5907 has a large ratio of mid-IR to near-IR flux density ($F(9\mu\mathrm{m})/F(Ks) = 11.1$). This mid-IR source is also coincident with a bright near-UV and optical source. We present photometries of AKARI J1757+5907 in table 1. The photographic magnitudes are from USNO-B1.0 catalog (Monet et al. 2003), and they are converted to $g, r$, and $i$ magnitude using equation 2 of Monet et al. (2003). We found the radio source NVSS J175659.82+590801.5 ($6.5 \pm 0.5$ mJy at 1.4 GHz) (Condon et al. 1998) is coincident with AKARI J1757+5907. The ratio of radio (5 GHz) to optical (4400 Å) flux density is 1.4 assuming radio spectral index is -0.5. The ratio indicates the quasar is radio quiet (Kellermann et al. 1989).

The follow-up spectroscopy using KPNO 2.1m telescope revealed that AKARI J1757+5907 is a $z = 0.615$ quasar that shows He I* and Mg II absorption lines as well as H$\beta$ and strong Fe II emission lines (Toba et al, in preparation). The spectrum resembles the one of QSO 2359-1241 (Brotherton et al. 2001; Arav et al. 2001). Both quasars show rare He I* absorption as well as Mg II absorption. They also have redder continua and strong Fe II emission lines. The high resolution spectroscopy of QSO 2359-1241 by Arav et al. (2001) revealed Fe II absorption lines, Thus Fe II absorption lines are expected to exist in AKARI J1757+5907. Following Korista et al. (2008), by measuring the ionic column densities ($N_{ion}$) of Fe II and He I*, we can constrain the ionization parameter ($U_H$) and hydrogen column density ($N_H$). The high brightness of this quasar permits us to do high resolution spectroscopy of He I* absorption lines and search for Fe II resonance and excited state absorption lines. The $N_{ion}$ ratio of Fe II* to Fe II(E=0) yields the hydrogen number density, which in turn yields the distance of outflowing gas from the central source, $\dot{E}_k$ and $\dot{M}_{out}$ by using the number density, $U_H$ and $N_H$.

The plan of this paper is as follows. In § 2 we describe the observations and data reduction. In § 3 we determine the redshift of the object. The outflow absorption troughs are discussed in § 4 and the spectral energy distribution in § 5. In § 6 we describe our photoionization modeling, and in § 7 the resultant determination of mass flow rate and kinetic luminosity for the outflow. In § 8 we discuss our results and in § 9 we describe the scientific potential of additional Subaru/HDS and HST/COS observations targeting this object. Throughout this paper we assume $H_0 = 70$ km s$^{-1}$ Mpc$^{-1}$, $\Omega_m = 0.3$, and $\Omega_\Lambda = 0.7$. Note that wavelengths of any transition in this paper are ones in vacuum, and the observed wavelength scale is converted to one in vacuum.

## 2. Observations and Data Reduction

### *2.1. high resolution spectroscopy*

The high resolution spectroscopy of AKARI J1757+5907 (R.A.=17:57:00.24, Decl.=+59:08:00.3 (J2000.0)) was done with the High Dispersion Spectrograph (HDS; Noguchi et al. 2002) attached to the Subaru 8.2 m telescope (Iye et al. 2004) on 2010 June 17 (UT). The weather conditions were poor with thick cirrus and the seeing was unstable (>1.″0). The slit width was set to be 1.″0. The HDS setting was Yd covering between 4054 and 6696 Å. This results in a resolving power of $R \sim 36000$. The binning was 2 (spatial direction) × 4 (dispersion direction). We obtained eight exposures of 1800 s each, however, one of them is unusable due to low signal-to-noise ratio.

The data were reduced using IRAF[1] for the standard procedures of overscan subtraction, dark subtraction, cosmic ray removal and flat-fielding, where wavelength calibration was performed using the Th-Ar lamp. the rms wavelength calibration error is 0.011 - 0.013 Å. The one-dimensional spectra were extracted from each exposure. Heliocentric correction was applied. After that, all the spectral exposures were combined, and all orders were connected to one spectrum. We normalized the spectrum using spline fits. Finally we converted to vacuum wavelength scale.

### *2.2. Spectrophotometry*

The low resolution spectrophotometry of AKARI J1757+5907 was done on 2010 June 30 (UT) with FOCAS (Kashikawa et al. 2002) attached to the Subaru telescope. The new fully-depleted-type CCDs developed by NAOJ/ATC and fabricated by Hamamatsu Photonics K. K. were installed and commissioned at that time. We obtained six spectra of 5 minutes integration under a clear condition and good seeing (0.″6 - 0.″9 ). The 2.″0 width slit was used for spectrophotometry purpose. We used two configurations: the R300 grism with the O58 filter ('red') and the B300 grism without any order-cut filters ('blue'). The first three 300s spectra were the 'red' which covers between 5700 Å and 10200 Å. The last three 300s spectra were the 'blue' which have an uncontaminated range between 3500 Å and 7000 Å. The atmospheric dispersion corrector was used. The slit position angle was 0°, and the binning was 2 (spatial direction) × 1 (dispersion direction) The spectrophotometric standard star BD+28°4211 was observed for sensitivity calibration.

The data were reduced using IRAF for the standard procedures of bias subtraction, wavelength calibration, and sky subtraction, except for flat-fielding. AKARI J1757+5907 is so bright that its counts on the CCD are comparable to the flat frames, and are much higher at shorter wavelength (< 4000 Å). The flat-fielding procedure significantly reduced its signal-to-noise

[1] IRAF is distributed by the National Optical Astronomy Observatory, which is operated by the Association of Universities for Research in Astronomy, Inc., under cooperative agreement with the National Science Foundation.

ratio. We therefore skipped the flat-fielding procedure. Wavelength calibration was performed using OH night sky emission lines for the red spectra and the Cu-Ar lamp for the blue ones. The rms error of wavelength calibration is 0.2 Å. The seeing was much smaller than the slit width, thus the resolution was determined by the seeing disk size. The resulting He I* 3889 absorption line is 13 Å width at 6260 Å. This value corresponds to the resolving power of 480 ($\sim 620$ km s$^{-1}$), which is similar to the resolution obtained with the 0.″8 width slit, and is consistent with the seeing size during our observations. The sensitivity calibration was performed as a function of wavelength. The flux of the blue and red spectra at the same wavelength agree within 1.6%. The foreground Galactic extinction of $E(B-V) = 0.043$ mag (Schlegel, Finkbeiner, & Davis 1998) was corrected.

## 3. Results of spectrophotometry

Figure 1 displays the low-resolution optical spectrum of AKARI J1757+5907. The spectrum shows strong absorption lines of Mg II and He I* as well as emission lines of Mg II, Fe II, H$\gamma$, H$\beta$, [O III]. In order to determine the systemic redshift of the quasar, we deblend the [O III] emission lines from the H$\beta$ and Fe II emission lines. As seen in figure 1, AKARI J1757+5907 has strong Fe II emission lines. However, the Fe II emission template around H$\beta$ derived from the spectrum of I Zw 1 (Aoki, Kawaguchi, & Ohta 2005) is not a good match to the Fe II emission in AKARI J1757+5907 (figure 2a). The intensity ratios among Fe II emission lines are different between these objects. Thus, we cannot use the Fe II emission template derived form the spectrum of I Zw 1.

Instead we fit the spectrum between 7662 Å and 8204 Å with a combination of Fe II $\lambda\lambda$4925, 5020, H$\beta$, and [O III] after subtraction of a power-law continuum. This power-law continuum is constructed by fitting at 6526-6544 Å and 8842-8891 Å. The H$\beta$ emission line is fitted with a combination of three Gaussians. We fit the [O III] doublet $\lambda\lambda$4960.3, 5008.2 with two sets of two Gaussians. The width and redshift are assumed to be the same for each set, and the intensity ratio is fixed to be 3.0. Fe II $\lambda\lambda$4925, 5020 are modeled by two Lorentzians with the same width and redshift. Their redshift is fixed to be the same as the strongest Gaussian component of the H$\beta$. The result of fitting is shown in figure 2b. We need a separate "red wing" of H$\beta$ to get a satisfactory fit. This component may be [O III] emission line. The derived redshifts and FWHMs are tabulated in table 2. The FWHM is corrected for the instrumental broadening by using the simple assumption: $\mathrm{FWHM_{true}} = (\mathrm{FWHM_{obs}^2} - \mathrm{FWHM_{inst}^2})^{1/2}$, where $\mathrm{FWHM_{obs}}$ is the observed FWHM of the line and $\mathrm{FWHM_{inst}}$ is an instrumental FWHM (620 km s$^{-1}$). The redshift of the red component of [O III] is $0.6150 \pm 0.0001$. The rest equivalent width of [O III] including both components is $9.9 \pm 0.3$ Å. This value is consistent with the [O III] strength in majority ($> 50$ %) of Mg II BAL quasars reported by Zhang et al. (2010). We also detect weak [O II] emission at 6023.4 Å, which corresponds to a redshift of 0.6155. We thus adopt $0.61525 \pm 0.00025$ as the systemic redshift of the quasar. The blue component of [O III] is blueshifted by 980 km s$^{-1}$ relative to the systemic redshift.

## 4. Absorption lines

In the HDS spectrum of AKARI J1757+5907, the absorption lines are not heavily blended. The identification is thus a straightforward task. We identify Mg II $\lambda\lambda$2976, 2803, He I* $\lambda$2945, $\lambda$3188, $\lambda$3889, Fe II $\lambda$2600, $\lambda$2586 as well as weaker absorption troughs from Mg I $\lambda$2852, He I* $\lambda$2829, and Ca II $\lambda\lambda$3934, 3969. The strong absorption lines such as the Mg II doublet and He I*$\lambda$3889 clearly show 9 distinct troughs, which span a velocity range from $-660$ to $-1520$ km s$^{-1}$. The trough at $-1000$ km s$^{-1}$ has the same outflow velocity as the blue component of the [O III] emission line. We show the absorption troughs from Mg II $\lambda\lambda$2976, 2803, He I* $\lambda$2945, $\lambda$3188, $\lambda$3889, and Fe II $\lambda$2600, $\lambda$2586 in figure 3. We do not detect an Fe II $\lambda$2612 absorption trough from the E=385 cm$^{-1}$ excited level, which has the largest oscillator strength of the Fe II* lines from this energy level, in our spectral range. We show the spectral region of Fe II $\lambda$2612 in the lower panel of figure 3.

### *4.1. Column Density Determinations*

Both the Mg II and He I* troughs span the full velocity range from $-660$ to $-1520$ km s$^{-1}$ and appear in all 9 distinct troughs (see Figure 3). There is self blending in the Mg II troughs at the velocity extremes, which does not affect the majority of the troughs. The He I* and Fe II troughs are free of any self blending. Of the 9 troughs, only three have corresponding absorption in Fe II. These are in the range of $-1050$ to $-800$ km s$^{-1}$ (see Figure 3). Thus, we concentrate on this velocity range for our measurements as the best photoionization constraints are achieved by contrasting He I* and Fe II column densities (see section 6; Korista et al. 2008; Arav et al. 2010).

To determine the ionic column densities, we rebin the data to 10 km s$^{-1}$ and use the velocity dependent apparent optical depth (AOD), covering factor ($C(v)$), and power-law fitting methods from Dunn et al. (2010; methods 1, 2, and 3 in their subsection 3.2) across the range of $-1050$ to $-800$ km s$^{-1}$.

The AOD methods assumes that the emission source is completely and homogeneously covered by the absorber, so that the optical depth ($\tau(v)$) at a given velocity is related to the normalized intensity via: $I(v) = \exp(-\tau(v))$. The covering factor method assumes that at a given velocity, a fraction $C(v)$ of the emission source is covered with a constant value of optical depth, while the rest of the source is uncovered. In order to for both $\tau(v)$ and $C(v)$ we use use at least two absorption lines from the same energy level of the same ion, and solve for $I(v)_j = 1 - C(v) + C(v)\exp(-\tau(v)_j)$, where $I_j$ is the normalized intensity of the absorption due to the $j$ transition in the same energy level. The ratio of different $\tau(v)_j$ are known from atomic physics and therefor the

set of equations is solvable. The power-law model assumes that the absorption gas inhomogeneously covers the background source. The optical depth is described by $\tau_v(x) = \tau_{max}(v)x^a$, where $x$ is the spatial dimension in the plane of the sky, $a$ is the power law distribution index and $\tau_{max}$ is the highest value of $\tau$ at a given velocity. In case of the power law model, $\tau$ is averaged over the spatial dimension x.

In order to convert $\tau$ in each model to column density we use

$$N(v) = 3.8 \times 10^{14} \frac{1}{f\lambda} \tau(v) (\mathrm{cm}^{-2}\mathrm{km}^{-1}\mathrm{s}),$$

where $\lambda$ is the wavelength of the line in Å, $f$ is the oscillator strength. We use the oscillator strengths from Fuhr & Wiese (2006) for the Fe II lines and values from the NIST Atomic Spectra Database (2010) for Mg II and He I*.

In Figure 4, we show the He I* troughs and column density determination from the three lines of He I* present in the HDS spectrum. The He I* lines are well separated, have no self blending, and we obtain consistent results with all three column density extraction methods. There are two velocity points where the $C(v)$ becomes nonphysical (i.e., negative or larger than 1.0), near $-930$ km s$^{-1}$ and at velocities lower than $-850$ km s$^{-1}$. This occurs because the two weaker lines are very shallow at these velocities and are thus consistent with the continuum level and dominated by the noise.

We show in Figure 5 the trough profiles and column density results for Mg II. Both the red and the blue doublet troughs are quite deep and therefore their level of saturation is model dependent. The $C(v)$ solution suggests a small level of saturation (only 40% larger column density than the AOD estimate), while the power-law result is three times higher. This is an inherent feature of the absorption models where in order to fit deep doublet troughs the power-law model requires a much greater column density than the $C(v)$ solution (see the case of the O VI doublet in the spectrum of Mrk 279, Arav et al. 2005). Since we do not have data for troughs from additional Mg II lines, we cannot determine which model is more physical.

There is a possibility that a narrow Mg II emission line fills the trough. As already noted early in this section, the blue component of [O III] has the velocity of -1000 km s$^{-1}$. The Mg II emission line from the same gas probably exists. We estimate the flux of Mg II emission line using the flux ratio of [O III] $\lambda$5008 to Mg II in Seyfert 2 galaxies, NGC 1068 (Kraemer et al. 1998) and Mrk 3 (Collins et al. 2005). The ratios vary along the physical position in the galaxies between 0.03 and 0.15, and average of extinction corrected ratios are 0.09, and 0.07 in NGC 1068 and Mrk 3, respectively. We also assume a 1:2 ratio for the Mg II doublet, and gaussians of the same width ($\sigma = 205$ km s$^{-1}$) as the [O III] emission line. This width corresponds to 3.0 Å at the Mg II observed wavelength of 4500 Å. The HDS spectrum before normalization is scaled to the low-resolution spectrum. The expected height of the Mg II emission line will be $\sim$13 % and $\sim$4% of the residual intensity at Mg II $\lambda$2796 and $\lambda$2803 trough, respectively. Thus, the real residual intensity may be smaller than the observed one. Therefore, we conclude that the Mg II column density can be much larger than the AOD or $C(v)$ determined values.

Finally, we show the result for Fe II troughs in Figure 6. Unlike Mg II and He I*, the Fe II troughs are both shallow and in a much lower signal-to-noise region of the spectrum (towards the short wavelength end of the detector). Due to this, we find that the weaker Fe II $\lambda$2587 line is only detected across three velocity bins. Using both the Fe II $\lambda$2600 and the Fe II $\lambda$2587 lines we calculate $N_{FeII}$ for both $C(v)$ and power-law methods for the three bins and include them in the integrated total. Due to a lack of detection of the $\lambda$2587 line, we use the $\lambda$2600 line to calculate the column density from the AOD method for the remaining points. We also checked the column density for Fe II using the covering factor of Mg II. The column density calculated in this fashion changed only by $\sim$10% as Mg II nearly fully covers the source ($C(v) \approx 0.9$) in this velocity range.

### *4.2. Column Density Limits on Fe II* Excited State Lines*

In order to help constrain the photoionization models in section 6, we estimate the column density limits for the Fe II* $\lambda$2612 and $\lambda$2757 lines from the 385 and 7955 cm$^{-1}$ energy levels, respectively. Neither line shows a detectable trough in the data. Therefore, we can use the trough profile of Fe II $\lambda$2600 to determine the relative optical depth and column density of these two energy levels (see Section 3.3 of Dunn et al. 2010). We find upper limits on the ionic column densities of (3.7 and 0.5) $\times 10^{12}$ cm$^{-2}$ for the 385 and 7955 cm$^{-1}$ energy levels, respectively.

## 5. Determination of the Spectral Energy Distribution

Our FOCAS spectrophotometry data and the GALEX photometry clearly show the flux drops at shorter wavelengths ($<$ 2000 Å in the rest frame) and indicate reddening by dust (figure 7). We must consider extinction for deriving the intrinsic spectral energy distribution (SED). First, we measured the continuum flux at four points where there are less Fe II emission contaminates. These four points and the GALEX photometry points are then shifted to the rest frame. We fit a reddened power-law to the continuum points. We adopted the index of the power-law continuum ($\alpha$; $f_\nu \propto \nu^\alpha$) of the LBQS composite, -0.36 measured by Vanden Berk et al. (2001). We adopt the SMC-type extinction law. The best fit gives us the color excess $E(B-V)$ of 0.18. The best fit of the reddened power-law continuum is shown in figure 7.

To estimate the distance to the outflow from the central source ($R$), we need to determine the flux of hydrogen ionizing photons that irradiates the absorber (see equation [1] below). Using the Mathews & Ferland (1987) SED, reddened to match the observed spectrum, we find that number of hydrogen ionizing photons emitted per second

by the reddened central source ($Q_H$) is $2.2\times10^{57}$ photons $s^{-1}$. Here we assumed that the reddening occur between the central source and the outflow, as is the case where the photons are attenuated by the edge of the putative AGN obscuring torus (see full discussion in Dunn et al. 2010). This assumption will also give us smaller values for the inferred $R$ and therefore conservative lower limits for $\dot{M}_{out}$ and $\dot{E}_k$. The $L_{Bol}$ for the dereddened, intrinsic spectrum is $3.7\times10^{47}$ erg $s^{-1}$.

## 6. Photoionization Modeling

Through photoionization modeling, reliable measurements of He I* and Fe II column densities provide accurate constraints on the total hydrogen column density, $N_H$, and the hydrogen ionization parameter,

$$U_H \equiv \frac{Q_H}{4\pi R^2 n_H c}, \quad (1)$$

where $R$ is the distance from the central source, $n_H$ is the total hydrogen number density, and $c$ is the speed of light. We use version c08.00 of the spectral synthesis code Cloudy, last described by Ferland et al. (1998), to model a plane-parallel slab of gas with constant hydrogen number density irradiated by a source continuum. We focus on the kinematic components spanning a velocity range from $-800$ km $s^{-1}$ to $-1050$ km $s^{-1}$ where we detect Fe II(0). In this velocity range, measurements of upper limits on the Fe II(E=385 $cm^{-1}$) and the Fe II(E=7955 $cm^{-1}$) yield upper limits of electron number density $n_e$, $10^{3.6}$ and $10^{3.8}$ $cm^{-3}$, respectively. We adopt the conservative value of an upper limit of $n_e \leq 10^{3.8}$ $cm^{-3}$, and assume $n_H \approx n_e$, which is valid within the ionized zone we are discussing. While the electron number density is well constrained from above, there are no diagnostics for a lower limit on $n_e$ in the data.

We begin investigation of the parameter space by using Cloudy's optimization mode to determine $N_H$ and $U_H$ for $n_H = 10^{3.8}$ $cm^{-3}$. The parameters $N_H$ and $U_H$ are varied and ionic column densities are computed for each set of parameters. Best fit values are determined by $\chi^2$ minimization for given tolerances in the measured ionic column densities. We adopt the measured ionic column densities determined by the partial covering method, and optimize to $N_{Fe\ II}$ and $N_{He\ I*}$, since these are the more robust measurements. The measured and model predicted column densities are presented in table 3. For solar abundances and the MF87 SED, as implemented by Cloudy[2], we find $\log U_H = -2.15$ and $\log N_H = 20.82$ yield good fits to the column densities of He I* and Fe II while $N_{Mg\ II}$ is overpredicted. However, as discussed in section 4, the Mg II troughs may be more saturated than the partial covering model suggests. A hydrogen ionization front, which we define as the position at which half of the total hydrogen is neutral (approximated by $N_H = 10^{23} U_H$), does not form in this solution although we are very close to it with $\log(N_H/U_H) = 22.96$.

[2] This SED differs from the MF87 SED by the addition of a submillimeter break at 10 $\mu$m.

Since the data do not provide a lower limit to the electron number density, we find other valid solutions by reducing $n_H$. When the hydrogen number density is reduced, the He I* population drops. This is due to the fact that He I* is populated by recombination of He II and the number of recombinations per unit time depends linearly on $n_e$. Therefore, $N_H$ must increase in order to provide enough He I* to be consistent with the measured value. Fe II becomes dominant near the hydrogen ionization front, while He I* drops off drastically at the front. Thus, solutions in this region of the slab have $U_H$ fixed by $N_{He\ I*}$ and the ratio $N_H/U_H$ fixed by $N_{Fe\ II}$. Due to the tight correlation of $N_H$ and $U_H$, all valid solutions have a similar ratio laying (nearly) on a straight line in the $N_H$-$U_H$ plane for number densities greater than $\sim 100$ $cm^{-3}$. At these densities, the slabs do not form a hydrogen ionization front. As we go to densities lower than $\sim 100$ $cm^{-3}$, a front forms, behind which Fe II and Mg II increase linearly with $N_H$.

In order to determine what effects choice of SED may have on $N_H$ and $U_H$, we compare results of the MF87 SED with results of a softer SED. The soft SED has an optical to X-ray spectral index $\alpha_{ox} = -1.5$ compared to the MF87 SED with $\alpha_{ox} = -1.4$ (with the convention $F_\nu = \nu^\alpha$) and was generated using the Cloudy command agn 375000 -1.50 -0.125 -1.00, where the numbers are the temperature of the UV bump, $\alpha_{ox}$, $\alpha_{uv}$, $\alpha_x$, respectively. We find the resulting $N_H$ and $U_H$ are nearly identical and conclude that changing the SED only affects the energetics through $Q_H$, a finding consistent with the analysis of QSO 1044+3656 reported in Arav et al. (2010).

Another assumption in our models is solar abundances. To check the sensitivity of our results to metallicity changes, we use the abundances in table 2 of Ballero et al. (2008) for metallicity Z=4.23 with the MF87 SED and $\log n_H = 3.8$. While helium abundances are expected to increase with oxygen abundances (e.g., Olive & Scully (1996)), the amount of increase varies for different galaxies. Therefore, to be conservative, we increase the helium abundance significantly to 15% above solar. We find that $\log U_H$ is approximately 0.02 dex lower and $\log N_H$ is approximately 0.15 dex lower for the increased metallicity model with $\log(N_H/U_H) = 22.83$. We discuss the effect of these changes on the energetics of the outflow in the next section.

## 7. Energetics of the Outflow

Of particular interest for any outflow are its mass ($M_{out}$), the average mass flow rate ($\dot{M}_{out}$) and mechanical work output or kinetic luminosity ($\dot{E}_k$). Assuming the outflow is in a form of a thin partial shell moving with a constant radial velocity ($v$), at a distance $R$ from the source, the mass of the outflow is:

$$M_{out} = 4\pi\mu m_p \Omega R^2 N_H, \quad (2)$$

where $N_H$ is the total column density of hydrogen, $m_p$ is the mass of a proton, $\mu$=1.4 is the plasma's mean molecular weight per proton, and $\Omega$ is the fraction of the shell

occupied by the outflow. The average mass flow rate is given by dividing the outflowing mass by the dynamical time scale of the outflow $R/v$ (see full discussion in Arav et al 2010), therefore

$$\dot{M}_{out} \sim \frac{M_{out}}{R/v} = 4\pi\mu m_p \Omega R N_H v \quad (3)$$

$$\text{and} \quad \dot{E}_k = \frac{1}{2}\dot{M}_{out}v^2 \sim 2\pi\mu m_p \Omega R N_H v^3. \quad (4)$$

For the troughs we consider in AKARI J1757+5907, the median velocity of the system is $-970$ km s$^{-1}$. We assume that $\Omega = 0.2$, which is the percentage of quasars showing BALs in their spectrum (see discussion in Dunn et al. 2010).

To determine the distance, we solve equation (1) for $R$, which depends on $U_H$ and $n_H$. The lack of Fe II* detection yields an upper limit of $n_H < 10^{3.8}$ cm$^{-3}$ (see Section 6), and therefore, as shown below, a lower limit on $R$.

For the range $10^{1.8} < n_H < 10^{3.8}$, our photoionization solutions obey the relationships $N_H \propto U_H$ and $U_H \propto n_H^{-\alpha}$, where $0.4 < \alpha < 1$ ($\alpha$ decreases as $n_H$ increases). The first relationship arises from the requirement of being close to a hydrogen ionization front, and the second is due to the decreasing electron population at the He I* meta stable level for lower number densities. Therefore, equation (1) yields $R \propto n_H^{(\alpha-1)/2}$. We use the solar abundances photoionization solution values from Section 6 ($\log U_H = -2.15$, $\log N_H = 20.82$ cm$^{-2}$ for $n_H = 10^{3.8}$ cm$^{-3}$) and $Q_H$ from Section 5. Inserting these values into equation (1), provides a lower limit on the distance, $R > 3.7$ kpc for $n_H = 10^{3.8}$ cm$^{-3}$, which only increases to 6.6 kpc for $n_H = 10^{1.8}$(cm$^{-3}$) due to the weak dependence of $R$ on $n_H$. From equation (3) we observe that $\dot{M}_{out}$ and $\dot{E}_k$ depend linearly on the product $RN_H$, which is proportional to $n_H^{-(1+\alpha)/2}$. Therefore, the upper limit for $n_H$ provides lower limit to $\dot{M}_{out}$ and $\dot{E}_k$. Using the $N_H$ and $R$ derived for $n_H = 10^{3.8}$ cm$^{-3}$, we find lower limits of $\dot{M}_{out} > 70$ $\Omega_{0.2}$ $M_\odot$ yr$^{-1}$ and $\dot{E}_k > 2.0 \times 10^{43}$ $\Omega_{0.2}$ ergs s$^{-1}$, where $\Omega_{0.2} \equiv \Omega/0.2$.

In the previous section, we discussed changes in $N_H$ and $U_H$ due to metallicity and SED changes. Using the Ballero et al. (2008) abundances for Z/Z$_\odot$=4.23 reduces the mass flow rate by $\sim 30\%$. Changing to the soft SED described in the previous section results in very small changes in $N_H$ and $U_H$, but $Q_H$ increases by a factor of $\sim 2$, increasing the mass flow rate by a factor of $\sim \sqrt{2}$.

The mass of the black hole ($M_{BH}$) of AKARI J1757+5907 is derived to be $4.0 \times 10^9 M_\odot$ based on the width of the H$\beta$ emission line of $\sigma = 2160$ km s$^{-1}$ and the dereddened optical luminosity $\lambda L(5100\text{Å})$ of $3.8 \times 10^{46}$ erg s$^{-1}$. We use the formula in Bennert et al. (2010) based on the calibrations of broad-line region size-luminosity relation (Bentz et al. 2006) and the virial coefficient taken from Onken et al. (2004). The derived $\log L_{bol}/L_{Edd} = -0.13$ is used for calculation of mass accretion rate ($\dot{M}_{acc}$) based on the accretion disk model by Kawaguchi (2003), which takes into account the effects of electron scattering (opacity and disk Comptonization) and the relativistic effects. The $\dot{M}_{acc}$ is 110 $M_\odot$ yr$^{-1}$, which is similar to the lower limit of $\dot{M}_{out}$.

We note that the $\Omega = 0.2$ we use is based the percentage of quasars showing C IV BALs. In a recent work, Dai et al. (2010) have shown that in the near infra-red surveys low ionization BALs (LoBALs) fraction is 4%, considerably higher than deduced from optical surveys (probably due to obscuration effects in the optical band). A more appropriate comparison in our case is to include somewhat narrower outflows with 1000 km s$^{-1}$ $< \Delta v <$ 2000 km s$^{-1}$. For these LoBALs based on "Absorption index" (Trump et al. 2006), Dai et al. (2010) find a 7.2% fraction. The frequency of He I* outflows is much less known. The strongest He I* line in the optical ($\lambda$3889) is shifted outside the optical range for objects where we can detect C IV $\lambda$1550 from the ground (e.g., z=1.5 for SDSS spectra), so a meaningful census of these outflows is difficult to come by. Anecdotally, we find that in most cases where we detect Fe II absorption trough, we also detect He I* troughs provided we have a clear spectral coverage of the latter (e.g., Arav et al. 2008; Arav et al. 2010).

We also point out that AKARI J1757+5907 as well as QSO 2359-1241 do not have measurable Fe II absorption in their low resolution spectra. Also, their outflow velocities ($\sim 1200$ km s$^{-1}$) and widths of troughs are moderate. Quasars with similar moderate outflows are more numerous than extreme FeLoBALs (e.g., SDSS J0318-0600, Hall et al. (2002)), and as we show here, can have similar mass flow rate and kinetic luminosity as the more extreme ones. This fact suggests the mass flow rate and kinetic luminosity values found here are more common among quasars, than judged by the rarity of extreme FeLoBALs. If we assume as a conservative limit that the $\Omega$ of the outflow seen in AKARI J1757+5907 is similar to the 7.2% LoBALs fraction found by Dai et al. (2010) then $\Omega_{0.2} = 0.36$, which will reduce the values for mass flow rate and kinetic luminosity accordingly.

## 8. Discussion

In Table 4 we show our $\dot{M}_{out}$ and $\dot{E}_k$ determinations in quasar BAL outflows to date (the older, less accurate, ones are shown in table 10 of Dunn et al 2010). While the lower limit on $\dot{E}_k$ for the AKARI J1757+5907 outflow is rather low for AGN feedback purposes, we note that the corresponding $\dot{M}_{out}$ value is large enough to yield a significant contribution for the metal enrichment of the intra-cluster medium around the parent galaxy (see Hallman and Arav 2010 [ApJ submitted])

We also note that this moderate velocity outflow is similar to those discovered in post-starburst galaxies at $z \sim 0.6$ (Tremonti, Moustakas, Diamond-Stanic 2007). Those galaxies show an outflow with Mg II absorption and a velocity of 1000 km s$^{-1}$ . Their stellar masses are as high as $(0.7 - 4.8) \times 10^{11} M_\odot$ (calculated from stellar population synthesis modeling fit to their spectra). For comparison, the $M_{BH}$ of AKARI J1757+5907 is $4.0 \times 10^9 M_\odot$, therefore based on $M_{BH}$-$M_{bulge}$ relation (Häring & Rix 2004), the bulge of its host galaxy is estimated

at $M_{bulge}1.8 \times 10^{12} M_{\odot}$. In addition, our derived $N_H$ is similar to the one Tremonti, Moustakas, Diamond-Stanic (2007) derived for outflow in the massive post-starburst galaxies ($N_H = 2 \times 10^{20}$ cm s$^{-1}$). They also pointed out that AGNs probably exist in those post-starburst galaxies because they get better fit to the spectra with a featureless blue power-law continuum and they detected high-excited emission-lines such as [O III] and [Ne V]. Thus, the outflows seen in the massive post-starburst galaxies may be same phenomena as outflows in quasars. These facts may be one of the indications that the outflow is a common phenomenon among massive galaxies. Tremonti, Moustakas, Diamond-Stanic (2007) had to make several assumptions to derive the physical quantities of the outflow because high resolution spectroscopy for such faint targets is difficult and non-detection of the important diagnostic absorption lines from Fe II (both ground and excited states) and He I*. In contrast, our high-resolution spectroscopy of BAL outflows in quasars, can constrain the total hydrogen column density and the distance of outflowing gas from the nucleus, which yield less model dependent estimates for $\dot{M}_{out}$ and $\dot{E}_k$.

## 9. Scientific gains with additional observations

### *9.1. Additional Subaru HDS data*

We expect data with a much higher signal-to-noise ratio using Subaru/HDS under good weather conditions. A half hour exposure should have a signal-to-noise ratio of 35 per pixel at 3800 Å where Fe II* $\lambda$2396 is shifted to. Our current upper limit to Fe II* $\lambda$2612 is derived from the data with signal-to-noise ratio of 30 per pixel. Fe II* $\lambda$2396 is 2.3 times stronger absorption than Fe II* $\lambda$2612. With two hours ($4 \times 1800$ sec) of exposure time, we expect five times more strict upper limit of the column density for the excited state of Fe II (385 cm$^{-1}$). Such an upper limit would translate to a hydrogen number density of $n_H < 10^{2.9}$ cm$^{-3}$. For this value of $n_H$ and our best model at that density ($\log U_H$ = -1.66 and $\log N_H = 21.32$), we find $R > 5.9$ kpc, $\dot{E}_k > 1.2 \times 10^{44}$ $\Omega_{0.2}$ ergs s$^{-1}$ and $\dot{M}_{out} > 340$ $\Omega_{0.2}$ $M_{\odot}$ yr$^{-1}$. It is of course possible that we'll be able to detect Fe II* $\lambda$2396 absorption, which will give us a determination of $n_e$ and therefore measurements (instead of lower limits) for $\dot{M}_{out}$ and $\dot{E}_k$.

In this paper our analysis focused on the troughs for which we can measure Fe II column density. The other six troughs have only upper limits for Fe II column density given the current signal-to-noise ratio. In order to study the relationship between the troughs, and obtain the integrated values of $\dot{M}_{out}$ and $\dot{E}_k$ for the full outflow, it is important to measure Fe II column density in all the troughs. Combined with our other measurements, this will constrain the ionization parameter and total hydrogen column density in each individual trough. We detect He I* absorption from 3 different lines in almost all the troughs (figure 3). The current data at He I* 2945, 3188 have a signal-to-noise-ratio of 65 per pixel. In order to get similar or better signal-to-noise ratio at Fe II resonance lines, 2383, 2586, and 2600, we will need two additional hours of HDS integration.

### *9.2. Imaging of outflowing gas*

The blue component of [O III] emission line has the same outflow velocity to the trough at $\sim 1000$ km s$^{-1}$. Furthermore, the derived density and ionization parameter values for the trough are typical for the narrow-line regions of AGNs (see, e.g., Groves, Dopita, Sutherland 2004). The scale of 3.7 kpc in AKARI J1757+5907 corresponds to 0.″55. The extended nebular gas associated with the outflow can be observed by the [O III] emission line by *HST* or the [S III] $\lambda$9533 emission line by integral filed spectroscopy coupled with adaptive optics observations from large ground-based telescopes. Currently, the solid angle subtended by the outflow is the parameter with the largest uncertainty. Imaging the outflowing gas will directly determine this parameter.

### *9.3. HST Cosmic Origins Spectrograph (COS) observations*

The near UV side of COS offers two important gains for the scientific investigation of the outflow in AKARI J1757+5907. First, using the G230L grating we can cover the full range of 1333–2800 Å (observed frame) with resolution of $\sim 3000$ and obtain data with S/N $\sim 30$ per resolution element using a total of six *HST* orbits. Such data will allow us to connect the low ionization absorption studied in this paper with the higher ionization phase seen in Si IV, C IV, and N V. In addition, this spectral range covers 3 pairs of Si II/Si II* lines that can determine number density considerably lower than is possible with the lines from the Fe II E=385 cm$^{-1}$ lines (essentially the critical density of the Si II* level is an order of magnitude lower than that of the Fe II E=385). In the unlikely event that we will detect Si II, but not Si II* absorption, which means that the gas density is substantially below the critical density for the Si II* level, we will have C II/C II* transitions covered that can determine the number density down to $n_e \sim 10$ cm$^{-3}$. These diagnostics practically guarantee that we will be able to determine $n_e$ and therefore the distance of the outflow, as long as $R < 100$ kpc.

In addition we can target the strongest pair of Si II/Si II* lines (1260 Å, 1265 Å) for a higher resolution ($R \sim 20{,}000$) in order to obtain a fully resolved trough where we can obtain $n_e$ as a function of velocity for all 9 outflow components. With 6 HST orbits using the COS 225M grating we can obtain high enough S/N to determine $n_e$ for 25-50 resolved velocity points across the full width of the outflow for a large dynamical range in $n_e$ ($100 < n_e < 3000$ cm$^{-3}$). This will allow for a sensitive tomography of the outflow and precise determination of the distance to each kinematic component.

We are grateful to the staff of Subaru Telescope especially T.-S. Pyo, and A. Tajitsu, for their assistance during our HDS observations. We thank T. Hattori for taking FOCAS spectra kindly and providing to us. We also thank Jong-Hak Woo, T. Kawaguchi and the ref-

eree for their helpful comments. This work was done when K. A. and K. T. K. were staying at the Physics Department of Virginia Tech in summer 2010. K. A. and K. T. K. thank the staff there for hospitality and support during their stay. We acknowledge support form NSF grant AST 0837880. This publication makes use of data products from the Two Micron All Sky Survey, which is a joint project of the University of Massachusetts and the Infrared Processing and Analysis Center/California Institute of Technology, funded by the National Aeronautics and Space Administration and the National Science Foundation.

## References

Aoki, K., Kawaguchi, T., & Ohta, K. 2005, ApJ, 618, 601
Arav, N., Brotherton, M. S., Becker, R. H., Gregg, M. D., White, R. L., Price, T., & Hack, W. 2001, ApJ, 546, 140
Arav, N., Kaastra, J., Kriss, G. A., Korista, K. T., Gabel, J., & Proga, D. 2005 ApJ, 620, 665
Arav, N., Moe, M., Costantini, E., Korista, K. T., Benn, C., & Ellison, S. 2008, ApJ, 681, 954
Arav, N., Dunn, J. P., Korista, K. T., Edmonds, D., González-Serrano, J. I., Benn, C., & Jiménez-Luján, F. 2010, submitting to ApJ
Ballero, S. K., Matteucci, F., Ciotti, L., Calura, F., & Padovani, P. 2008, A&A, 478, 335
Barlow, T. A. & Sargent, W. L. W. 1997, AJ, 113, 136
Bautista, M. A., Dunn, J. P., Arav, N., Korista, K. T., Moe, M., & Benn, C. 2010, ApJ, 713, 25
Brotherton, M. S., Arav, N., Becker, R. H., Tran, H. D., Gregg, M. D., White, R. L., Laurent-Muehleisen, S. A., & Hack, W. et al. 2001, ApJ, 546, 134
Bennert, V. N., Treu, T., Woo, J.-H., Malkan, M. A., Auger, M. W., Gallagher, S., & Blandford, R. D. 2010, ApJ, 708, 1507
Bentz, M. C., Peterson, B. M., Pogge, R. W., Vestergaard, M., & Onken, C. A. 2006, ApJ, 644, 133
Brüggen, M. & Scannapieco, E. 2009, MNRAS, 398, 548
Ciotti, L., Ostriker, J. P., & Proga, D. 2010, ApJ, 717, 708
Collins, N. R., Kraemer, S. B., Crenshaw, D. M., Ruiz, J., Deo, R., & Bruhweiler, F. C. 2005, ApJ, 619, 116
de Kool, M., Arav, N., Becker, R. H., Gregg, M. D., White, R. L., Laurent-Muehleisen, S. A., Price, T., & Korista, K. T. 2001, ApJ, 548, 609
Condon, J. J., Cotton, W. D., Greisen, E. W., Yin, Q. F., Perley, R. A., Taylor, G. B., & Broderick, J. J. 1998, AJ, 115, 1693
Dai, X., Shankar, F. and Sivakoff, G. R., arXiv:1004.0700
de Kool, M., Becker, R. H., Arav, N., Gregg, M. D., White, R. L. 2002, ApJ, 570, 514
Di Matteo, T., Springel, V., & Hernquist, L. 2005, Nature, 433, 604
Dunn, J. P. et al. 2010, ApJ, 709, 611
Ferland, G. J., Korista, K. T., Verner, D. A., Ferguson, J. W., Kingdon, J. B., Verner, E. M. 1998, PASP, 110, 761
Fuhr, J., & Wiese, W. 2006, J. Phys. Chem. Ref. Data, 35, 1669
Ganguly, R., & Brotherton, M. S. 2008, ApJ, 672, 102
Groves, B. A., Dopita, M. A., Sutherland, R. S. 2004, ApJS, 153, 9
Hall, P. B., et al. 2002, ApJS, 141, 267
Hamann, F. W., Barlow, T. A., Chaffee, F. C., Foltz, C. B., & Weymann, R. J. 2001, ApJ, 550, 142
Häring, N.,& Rix, H.-W. 2004, ApJL, 604, L89
Hewett, P. C. & Foltz, C. B. 2003, AJ, 125, 1784
Hopkins, P. F., Hernquist, L., Cox, T. J., & Kerěs, D. 2008, ApJS, 175, 356
Ishihara, D., et al. 2010, A&A, 514, A1
Iye, M., et al. 2004, PASJ, 56, 381
Kashikawa, N., et al. 2002, PASJ, 54, 819
Kawaguchi, T. 2003, ApJ, 593, 69
Kellermann, K. I., Sramek, R., Schmidt, M., Shaffer, D. B., & Green, R. 1989, AJ, 98, 1195
Knigge, C., Scaring, S., Goad, M. R., & Cottis, C. E. 2008, MNRAS, 386, 1426
Korista, K. T., Bautista, M., A., Arav, N., Moe, M., Costantini, E., & Benn, C. 2008, ApJ, 688, 108
Kraemer, S. B., Ruiz, J. R., & Crenshaw, D. M. 1998, ApJ, 508, 232
Mathews, W. G. & Ferland, G. J. 1987, ApJ, 323, 456
Moe, M., Arav, N., Bautista, M., A., & Korista, K. T. 2009, ApJ, 706, 525
Moll, R., et al., 2007, A&A, 463, 513
Monet, D., G., et al. 2003, AJ, 125, 984
Murakami, H., et al., 2007, PASJ, 59, 369
Noguchi, K., et al. 2002, PASJ, 54, 855
Olive, K. A. & Scully, S. T. 1996, International Journal of Modern Physics A, 11, 409
Onken C. A., Ferrarese, L., Merritt, D., Peterson, B. M., Pogge, R. W., Vestergaard, M., & Wandel A. 2004, ApJ, 615, 645
Schlegel, D. J.,Finkbeiner, D. P., & Davis, M. 1998, ApJ, 500, 525
Skrutskie, M. F., et al. 2006, AJ, 131, 1163
Tremonti, C. A., Moustakas, J., & Diamond-Stanic, A. M. 2007, ApJL, 663, L77
Trump, J. et al. 2006, ApJS, 165,1
Vanden Berk, D. E. et al., 2001, AJ, 122, 549
Wampler, E. J., Chugai, N. N., & Petitjean, P. 1995, ApJ, 443, 586
Weymann, R. J., Morris, S. L., Foltz, C. B., & Hewett, P. C. 1991, ApJ, 373, 23
Zhang, S., Wang, T.-G., Wang, H., Zhou, H., Dong, X.-B. & Wang, J.-G., ApJ, 714, 367

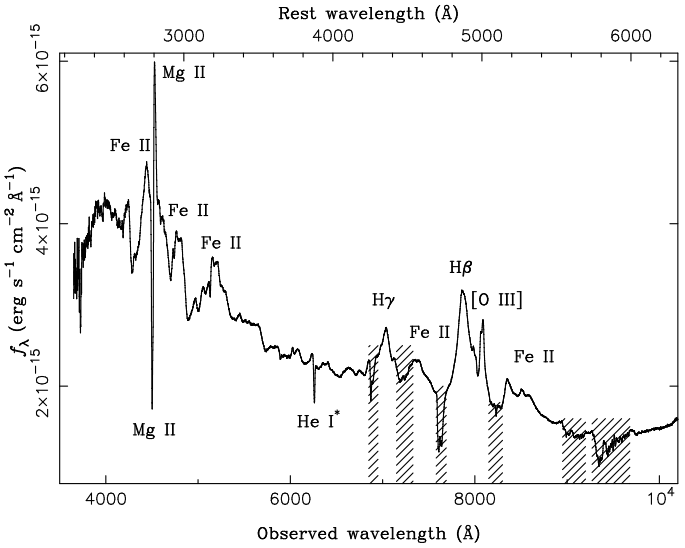


**Fig. 1.** Low resolution spectrum of AKARI J1757+5907. Ordinate is a flux density corrected for the Milky Way extinction in units of erg s$^{-1}$ cm$^{-2}$ Å$^{-1}$, and abscissa is the observed wavelength in angstrom. The rest wavelength is given along the top axis. The hatched regions indicate the place of telluric absorption.

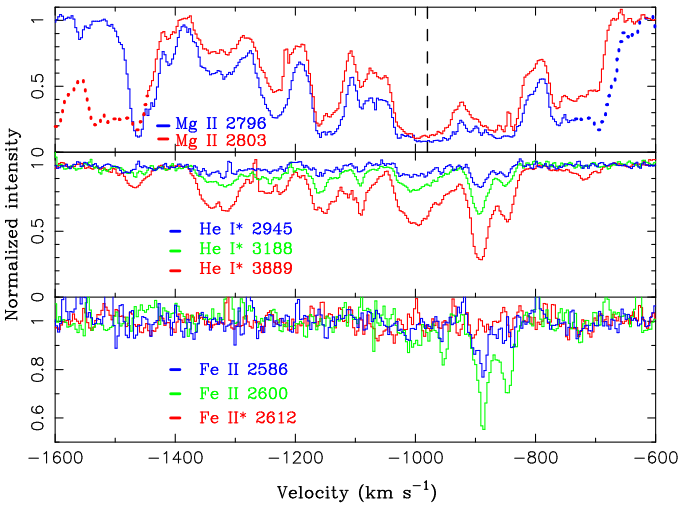


**Fig. 3.** Outflow troughs in AKARI J1757+5907. Ordinate is a normalized flux density, and abscissa is velocity from the systemic redshift ($z = 0.61525$). Blended parts are denoted as dotted spectra. The dashed vertical line indicates the position of the blue component of [O III] emission line. The velocity of that [O III] corresponds to the trough at $\sim -1000$ km s$^{-1}$.

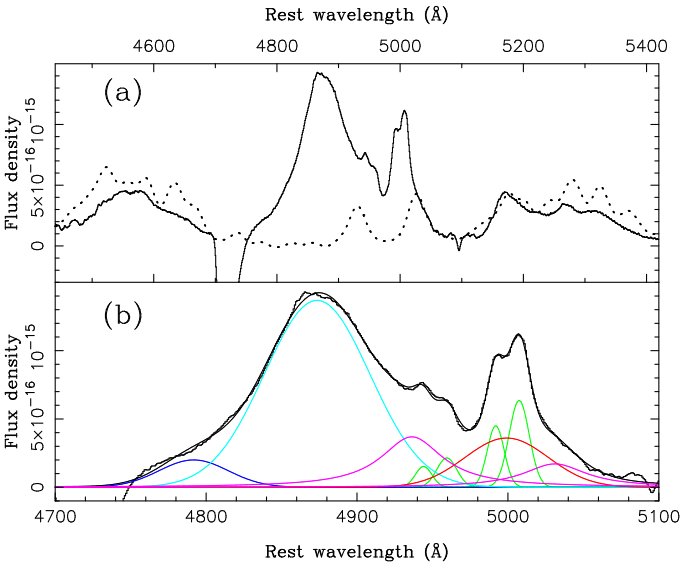


**Fig. 2.** The H$\beta$-[O III] region of AKARI J1757+5907. (a) Continuum subtracted spectrum. The dotted line is the Fe II template produced from I Zw 1. The Fe II template is broadened and scaled at 5170 Å. Note that the Fe II template is clearly different from Fe II emission line of AKARI J1757+5907 at 4600-4700 Å and 5260-5400 Å. (b) Fit of the spectrum. H$\beta$, [O III] doublet, and Fe II $\lambda\lambda$4925, 5020 are fitted with a three Gaussians (cyan, blue and red lines), two sets of two Gaussians (green lines), and two Lorentzians (magenta lines), respectively.

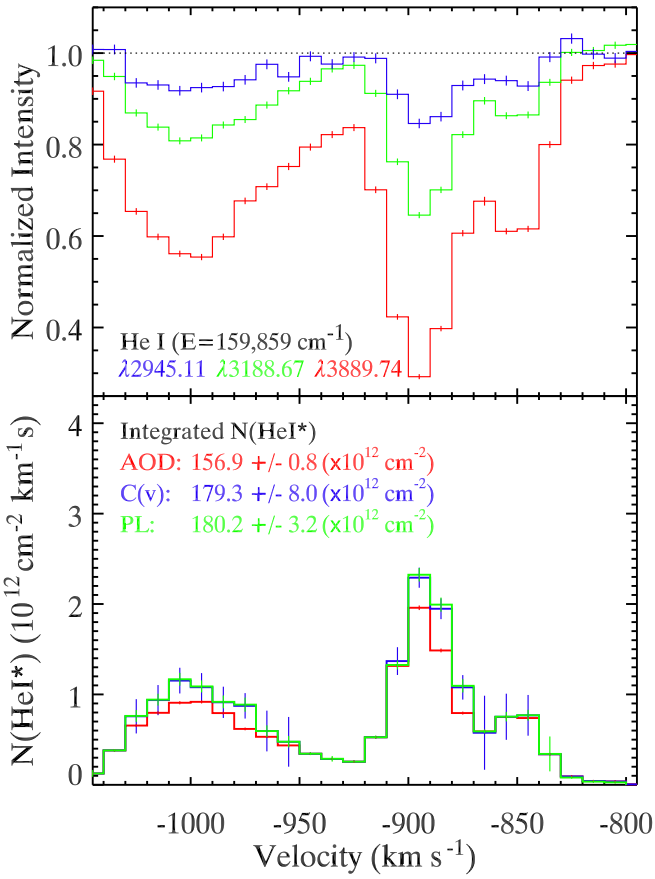


**Fig. 4.** Top: Absorption troughs from He I $\lambda$3890, 3190, and 2946 as red, green, and blue histograms, respectively. Vertical bars represent the statistical uncertainties in the residual intensity. Bottom: Velocity-dependent column density determinations for He I* from the AOD (red histograms), $C(v)$ (blue histograms), and power-law (green histograms) solutions. The velocity-integrated He I* column density values for the three methods and their associated statistical uncertainties are also listed.

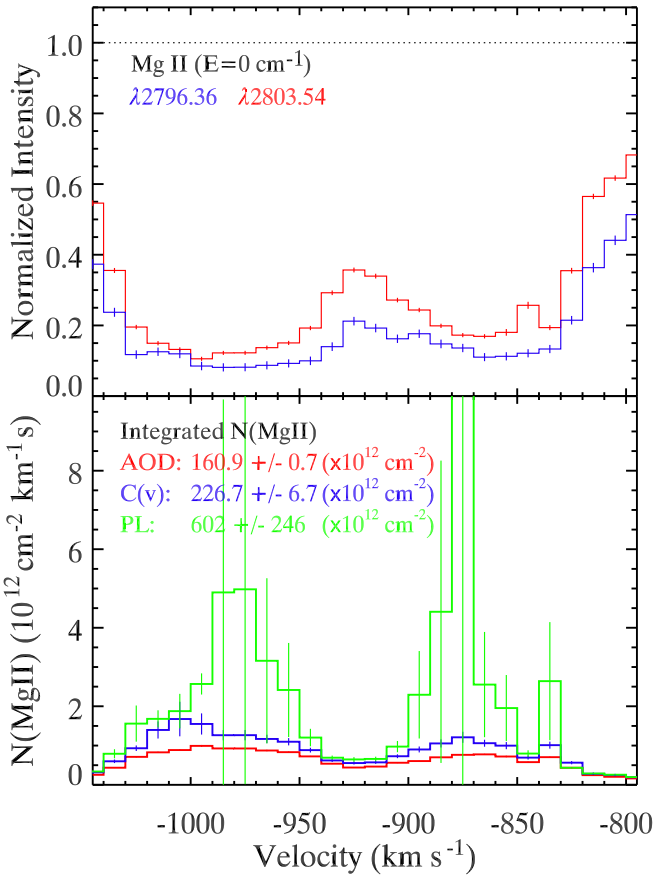


**Fig. 5.** Similar to Figure 4. Top: This shows the trough profiles for the Mg II doublet lines $\lambda\lambda$2796, 2804 (blue and red histograms, respectively) and their associated statistical uncertainties. Velocity-dependent column density determinations from the AOD (red histograms), $C(v)$ (blue histograms), and power-law (green histograms) solutions. The velocity-integrated column density values for the three methods and their associated statistical uncertainties are also listed.

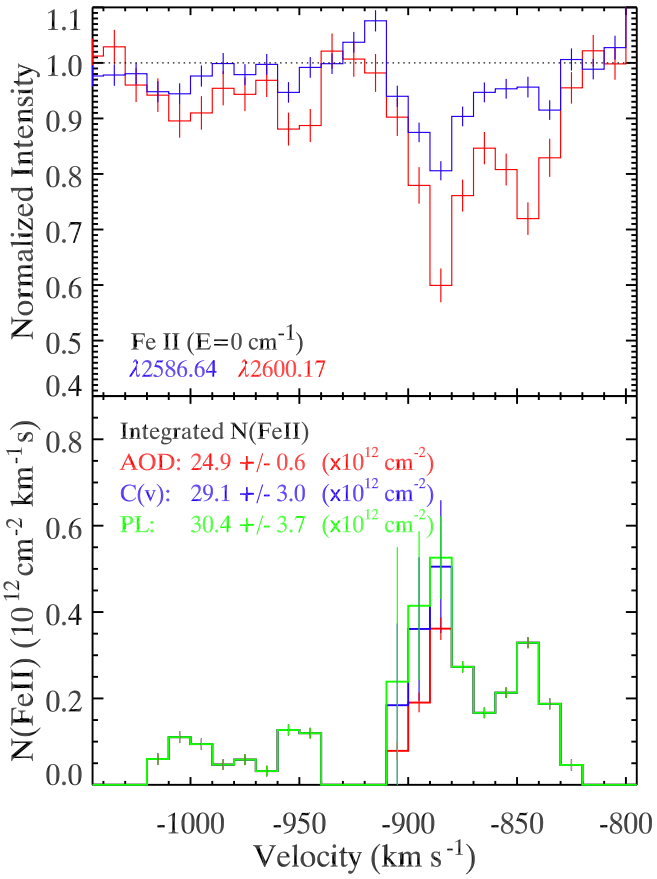


**Fig. 6.** Similar to Figures 4 and 5. Top: The trough profiles for the Fe II λ2600 and 2587 lines as red and blue histograms, respectively. Their associated statistical uncertainties are shown as vertical slashes. Bottom: The AOD, $C(v)$, and power-law column densities plotted as a function of velocity and the respective integrated values in red, blue, and green, respectively.

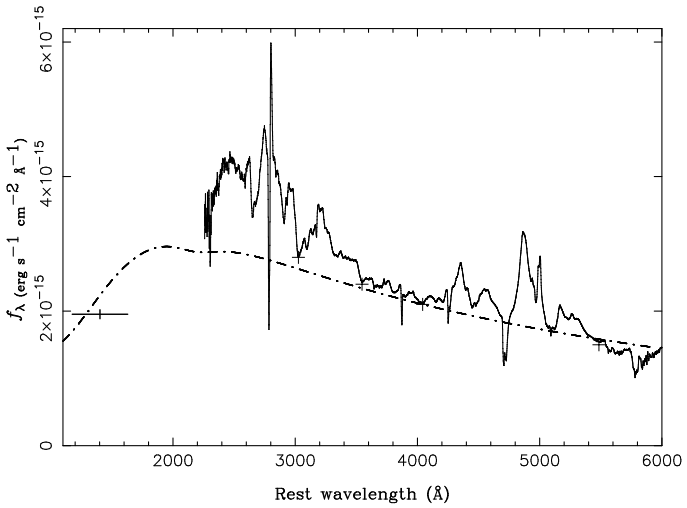


**Fig. 7.** Reddening of AKARI J1757+5907. Ordinate is a flux density corrected for the Milky Way extinction in units of erg $s^{-1}$ $cm^{-2}$ $Å^{-1}$ and abscissa is a rest wavelength. The rest optical spectrum is shown with the GALEX photometry (the most left cross) and continuum measurements (four crosses) from our spectrum. The power-law continuum reddened by the SMC-type extinction law with $E(B-V) = 0.18$ is shown with a dot-dashed line.

**Table 1.** Photometry of AKARI J1757+5907.

| Source | Band | flux density/magnitude |
|---|---|---|
| GALEX | NUV | $230.55 \pm 8.03 \mu$Jy* |
| POSS-I | $g$ | 15.1 mag. |
| POSS-I | $r$ | 15.0 mag. |
| POSS-II | $g$ | 15.2 mag. |
| POSS-II | $r$ | 15.3 mag. |
| POSS-II | $i$ | 15.1 mag. |
| 2MASS | $J$ | $13.728 \pm 0.021$ mag. |
| 2MASS | $H$ | $13.074 \pm 0.024$ mag. |
| 2MASS | $K_s$ | $12.344 \pm 0.023$ mag. |

*This value corresponds to $(1.345 \pm 0.047) \times 10^{-15}$ erg s$^{-1}$ cm$^{-2}$ Å$^{-1}$ at 2267 Å.

**Table 2.** Properties of emission lines of AKARI J1757+5907.

| Line | $\lambda_{\rm obs}$ Å | $z$ | FWHM$_{\rm true}$ km s$^{-1}$ |
|---|---|---|---|
| H$\beta$ | 7872.0 | 0.6189 | 5080 |
| [O III] 5008.24 | 8088.3 | 0.6150 | 710 |
| [O III] 5008.24 | 8063.3 | 0.6100 | 480 |

**Table 3.** Measured and model predicted column densities

| Measurement Method / Model parameter | | | | | $N_{He\ I*}$* | $N_{Fe\ II(0)}$* | $N_{Mg\ II}$* |
|---|---|---|---|---|---|---|---|
| Measurements | | | | | | | |
| Apparent Optical Depth | | | | | 156.9 ±0.8 | 24.9 ±0.6 | 160.9 ±0.7 |
| Covering factor | | | | | 179.3 ±8.0 | 29.1 ±3.0 | 226.7 ±6.7 |
| Power Law | | | | | 180.2 ±3.2 | 30.4 ±3.7 | 602 ±246 |
| Models | | | | | | | |
| SED | Z/Z$_\odot$ | log $N_H$ | log $U_H$ | log $n_H$ | | | |
| MF87 | 1.00 | 20.82 | -2.15 | 3.8 | 176.5 | 30.9 | 1341.5 |
| Soft | 1.00 | 20.81 | -2.15 | 3.8 | 180.5 | 32.4 | 1364.6 |
| MF87 | 4.23 | 20.66 | -2.17 | 3.8 | 172.3 | 31.2 | 1815.5 |

*in units of $10^{12}$ cm$^{-2}$

**Table 4.** Properties of Measured Outflows to Date

| Object | log $L_{Bol}$ (ergs s$^{-1}$) | $R$ (kpc) | log $N_H$ (cm$^{-2}$) | log $U_H$ | log $\dot{E}_k$* (ergs s$^{-1}$) | $\dot{M}^*_{out}$ ($M_\odot$ yr$^{-1}$) | Reference† |
|---|---|---|---|---|---|---|---|
| AKARI J1757+5907 | 47.57 | $> 3.7$ | $> 20.82$ | $> -2.15$ | $> 43.30$ | $> 70$ | 1 |
| QSO 1044+3656 | 46.84 | $1.7 \pm 0.4$ | $20.84 \pm 0.10$ | $-2.19 \pm 0.10$ | $44.81\ ^{+0.09}_{-0.11}$ | $120 \pm 25$ | 2 |
| QSO 2359−1241 | 47.67 | $3.2\ ^{+1.8}_{-1.1}$ | $20.56 \pm 0.15$ | $-2.40 \pm 0.15$ | $43.36 \pm 0.27$ | $90\ ^{+35}_{-20}$ | 3 |
| SDSS J0838+2955 | 47.53 | $3.3\ ^{+1.5}_{-1.0}$ | $20.80 \pm 0.28$ | $-1.95 \pm 0.21$ | $45.35\ ^{+0.23}_{-0.22}$ | $300\ ^{+210}_{-120}$ | 4 |
| SDSS J0318−0600 | 47.69 | $5.9 \pm 0.4$ | $19.90 \pm 0.17$ | $-3.08 \pm 0.05$ | $44.55\ ^{+0.10}_{-0.15}$ | $60 \pm 20$ | 5 |

*Calculated using equation (3) assuming $\Omega = 0.2$. The values for the last three objects are half of those founds in the reference due to the use of an improved estimate for $M_\odot$ and $\dot{E}_k$ given by equation (3), over those given by equations (9) and (10) in Dunn et al. (2010).
† 1-This Work, 2-Arav et al. (2010), 3-Korista et al. (2008) & Bautista et al. (2010), 4-Moe et al. (2009), 5-Dunn et al. (2010)